

Spectroscopy of band-to-band optical transitions in Si-Ge alloys and superlattices

T. P. Pearsall,* L. Colace,† and Adam DiVergilio

Department of Electrical Engineering, University of Washington, Seattle, Washington 98195

W. Jäger‡

Mikrostrukturanalitik, Technische Fakultät, Universität Kiel, Kaiserstrasse 2, D-24143 Kiel, Germany

D. Stenkamp‡

Institut für Werkstoffwissenschaften VII, Universität Erlangen-Nürnberg, D-91058 Erlangen, Germany

Georgios Theodorou

Department of Physics, Aristotle University, Gr-54006, Thessaloniki, Greece

Hartmut Presting

Daimler Benz Research, D-89081 Ulm, Germany

Erich Kasper

Institut für Halbleitertechnik, University of Stuttgart, D-70174 Stuttgart, Germany

Klaus Thonke

Abteilung Halbleiterphysik, University of Ulm, Albert-Einstein-Alle 45, D-89069 Ulm, Germany

(Received 27 May 1997; revised manuscript received 31 October 1997)

We report the results of an extensive study of band-to-band optical transitions in Si-Ge ($n:m$) superlattices and alloys where $n \approx m$. Our samples were grown by molecular-beam epitaxy on (001) silicon using symmetrically strained layers and characterized by high-resolution x-ray diffraction and transmission electron microscopy. This growth procedure permits the synthesis of continuous Si-Ge superlattices with a thickness of several thousand Å. Optical absorption was studied by photocurrent spectroscopy at 300, 77, and 4.2 K. These results were analyzed to determine the dependence of the photocurrent on the photon energy. The energy dependence of absorption was also measured by optical transmission spectroscopy. Analysis of these experiments gives approximate agreement with photoconductivity experiments on the value of the energy gap, but also shows that the energy dependence of the absorption coefficient varies linearly with the photon energy, while photoconductivity experiments show that the photocurrent increases with the fourth power of the energy. The absorption coefficient, and its dependence on the photon energy, are calculated directly from the joint density of states which is extracted from the electronic band structure. Our calculations show that the dependence of optical absorption on photon energy is linear for perfect superlattices: $\alpha(\hbar\omega) = A_0(\hbar\omega - E_g)^x$, where $x = 1$, with the exponent increasing above 1 in the presence of disorder such as from atomic steps, interface roughness, and similar defects. [S0163-1829(98)06715-0]

I. INTRODUCTION

Si-Ge semiconductors are being used to create high-performance bipolar transistors and integrated circuits,^{1,2} highly integrated focal-plane array infrared detectors,³ and infrared light-emitting diodes.⁴ This progress demonstrates considerable promise for Si-based high-speed, low-power electronic, and optoelectronic devices.^{5,6} The development of efficient, high-speed electroluminescent diodes is based on the discovery that short-period ($\Lambda < 20$ interatomic distances) Si-Ge superlattices have a quasidirect band gap formed by folding the band structure by the superlattice period potential. Numerous theoretical band-structure calculations of these Si-Ge superlattice structures have established that new band-edge states are formed at $\mathbf{k}=0$, and that the optical matrix element between the top of the valence band and these new states is enhanced by several orders of magnitude

over that of the optical matrix element for the lowest indirect transition. These calculations also show that the optical matrix element at $\mathbf{k}=0$ remains at least one order of magnitude less than that observed in a direct-gap semiconductor such as GaAs.⁷

In principle, the direct or indirect character of the fundamental band gap can be determined from the measurement of the optical-absorption coefficient versus photon energy. This dependence is expressed

$$\alpha(\hbar\omega) = \frac{4\pi^2\hbar c}{V} \int W(E)\mathcal{N}(E)dE, \quad (1)$$

where $W(E)$ is the transition probability and $\mathcal{N}(E)$ is the joint density of states.⁸ In a direct-gap material, each state in the valence band is connected with one state in the conduction band because $\mathbf{k}_f - \mathbf{k}_i = 0$, leading to simple integration of Eq. (1). In the case of an indirect gap material, \mathbf{k}_f is con-

TABLE I. A summary of sample structures used in this work. All samples have been prepared to have the same average composition: 50% Si and 50% Ge. In most cases the buffer thickness is less than 10% of the superlattice thickness.

Sample	Type	Superlattice		Buffer		Cap		Substrate
		comp	thick. (nm)	comp.	thick. (nm)	comp.	thick. (nm)	
<i>B1585</i>	Alloy	Si _{0.5} Ge _{0.5}	200	Si _{0.25}	20	Si	10	$p^+ 10^{19}$
<i>B1590</i>		2:2	202	Si _{0.25}	20	Si	10	$p^+ 10^{19}$
<i>B1589</i>		4:4	200	Si _{0.25}	20	Si	10	$p^+ 10^{19}$
<i>B1587</i>		8:8	202	Si _{0.25}	20	Si	10	$p^+ 10^{19}$
	Bulk Si	—	—	—	—	—	—	—
<i>B2208</i>		4:4	196	Si _{0.25}	20	Si	1	$p^- < 10^{14}$
<i>B2209</i>		5:5	207	Si _{0.25}	20	Si	1	$p^- < 10^{14}$
<i>B2210</i>		6:6	244	Si _{0.25}	20	Si	1	$p^- < 10^{14}$
<i>B2211</i>	Alloy	Si _{0.5} Ge _{0.5}	193	Si _{0.25}	20	Si	1	$p^- < 10^{14}$
<i>B2212</i>		4:4	212	Si _{0.25}	50	Si _{0.5}	100	$p^+ 10^{19}$
<i>B2213</i>		5:5	254	Si _{0.25}	50	Si _{0.5}	100	$p^+ 10^{19}$
<i>B2214</i>		5:5	254	Si _{0.25}	1000	Si _{0.5}	100	$p^+ 10^{19}$
<i>B2215</i>		6:6	287	Si _{0.25}	50	Si _{0.5}	100	$p^+ 10^{19}$

nected by the phonon momentum \mathbf{k}_p to a multiplicity of initial states leading to a different dependence of the optical absorption coefficient on energy when Eq. (1) is integrated.

Most semiconductors have a near-gap band structure that can be approximated by a simple parabolic $E - \mathbf{k}$ relationship. For the purposes of optical absorption, this approximation can be used also to describe valence band because the heavy-hole band has a much larger density of states than the light-hole band, and so it dominates the absorption process. In this case, Eq. (1) can be evaluated explicitly for both direct transition absorption and indirect transition absorption:

$$\text{Direct band gap: } \alpha(\hbar\omega) = A(\hbar\omega - E_g)^{1/2}, \quad (2)$$

$$\text{Indirect band gap: } \alpha(\hbar\omega) = B(\hbar\omega - E_g)^2. \quad (3)$$

Equation (2) can be applied to the study of GaAs or InP, while Eq. (3) applies to Si and Si-Ge random alloy materials. However, neither equation can be applied to Si-Ge short-period superlattices. The near-edge band structure of the conduction band does not satisfy the basic simplifying assumptions leading to Eq. (2) and (3) because there are several nearly degenerate and nonparabolic branches of the conduction band near the band edge.^{9,10}

The near-edge valence-band structure of a Si-Ge short-period superlattice still resembles that of Si or GaAs. This similarity persists because there are no additional zone-edge states with energy near the top of the valence band. While the superlattice potential will cause a zone folding of the band structure to occur, the new states lie at energies of several hundred meV below the top of the valence band. Hence they do not play a role in our experiments. However, the same situation does not hold for the conduction band. Here the effect of zone folding is to produce several nearly degenerate states at the band edge. The $E - \mathbf{k}$ relationship for these states is not parabolic over an energy range comparable to a phonon energy, and hence there is no longer a simple expression for the dependence of the density of states on energy. However, Eq. (1) is still valid. That is, the optical-

absorption coefficient can be derived from the density of states. As a result, the functional form of the absorption coefficient can be expressed

$$\alpha(\hbar\omega) = C(\hbar\omega - E_g)^x, \quad (4)$$

where x is to be determined. In our study we have characterized optical absorption in Si-Ge alloys and superlattices by both photocurrent spectroscopy and by optical transmission spectroscopy. These results are compared to the theoretical determination of the density of states and the optical-absorption coefficient and their dependence on photon energy. Here we present the results of these measurements and calculations.

II. SAMPLE PREPARATION AND ANALYSIS

A. Sample structure and composition

All samples used in this work were grown by solid-source molecular-beam epitaxy (MBE) on Si(001) substrates. A critical feature of the sample structure is the incorporation of a partially strain-relaxed S_{0.25}Ge_{0.75} alloy buffer layer. The thickness of the Ge-rich buffer is designed so that the relief of the strain imposed by the Si substrate leads to a partially strained, and thus partially relaxed layer with an effective lattice parameter equal to that of an unstrained Si_{0.5}Ge_{0.5} alloy. This buffer is used as a ‘‘virtual substrate’’ for the nucleation and epitaxy of Si-Ge ($n:n$) superlattices. In these superlattices, the Si layers are strained in extension in the plane of the superlattice, while the Ge layers are strained in compression. (see Table I). This alternation of compression and strain leads to a symmetrically strained superlattice.¹¹ The critical layer thickness for this superlattice structure is much larger than the superlattice thicknesses ($2000 \text{ \AA} < t < 15\,000 \text{ \AA}$) grown for these experiments. We are using this technique of epitaxy that produces a superlattice with symmetric strain to produce continuous strained-layer superlattices with an extended well-defined layering of Si and Ge layers only a few atoms in thickness. The total superlattice thickness is large enough to enable measurements of electri-

Substrate	Buffer	Buffer	Superlattice	Cap	Cap
Si	Si	$\text{Si}_{0.25}\text{Ge}_{0.75}$	Si_nGe_n	Si	Si
$p+ : 10^{18}$	undoped	$n- :$	$n : 10^{17}$	$n : 10^{17}$	$n+ : 10^{20}$
	20 nm	20 nm	200 nm	1 nm	9 nm

FIG. 1. Schematic structure of the buffer and epitaxial layers in our samples. Layer thicknesses and dopings vary from one sample to another, but the thickness of the Si-Ge alloy buffer layer is always much less than that of the superlattice layer.

cal and optical properties characteristic of synthetic crystals based on the unit cell symmetry that is imposed during crystal growth. For the series *B1585–B1590*, the growth temperature of the silicon substrate was maintained at 450 °C during the growth of the buffer and the superlattice. A Sb surfactant was employed in order to suppress Ge segregation which tends to perturb the superlattice periodicity. During growth of the *B2212–2214* series, the temperature of the silicon substrate during growth was fixed at 450 °C for the buffer layers and at 320 °C for the superlattice. The superlattice in these samples is doped *p*-type using B coevaporation. The Sb surfactant in these films is employed only during the final 10% of the superlattice layer thickness. This lower growth temperature would preserve the superlattice periodicity at the cost of a possibly elevated level of vacancies or interstitial defects in these samples.

The sample structure for the *B1585–B1590* series of superlattices used for photoconductivity experiments is shown in Fig. 1. Note that the total thickness of the alloy buffer layer is much less than that of the superlattice. This relationship assures that the superlattice dominates the optical absorption. An exception is *B2214*, where the buffer thickness is much larger than the superlattice thickness.

B. Structural analysis by transmission electron microscopy and x-ray diffraction

Analytical and high-resolution transmission electron microscopy (TEM) of [110] cross-section samples were used for a comprehensive structural characterization of short-period Si-Ge (*m:n*) superlattices grown by low-temperature MBE on different Si-Ge alloy buffers deposited on Si(001) substrates. Detailed information about superlattice periodicity, interface sharpness, strain distribution, and average composition were obtained. Local average compositions of the superlattices were determined by energy-dispersive x-ray spectroscopy. The microstructural investigations were performed at an electron energy of 400 keV (JEOL 4000EX/FX). Electron transparent samples were prepared by mechanical polishing and subsequent Ar-ion milling on a liquid-nitrogen-cooled-stage.

The results of this examination were used to measure the periodicity and thickness, and to evaluate the interfacial roughness of the superlattices used in the optical study. High-resolution lattice images of these structures reveal that the interfaces between the individual Si and Ge layers are coherent, indicating pseudomorphic growth.¹² Figure 2 shows superlattice reflections visible up to the second order in a [110] diffraction pattern taken from the sample *B2215*.

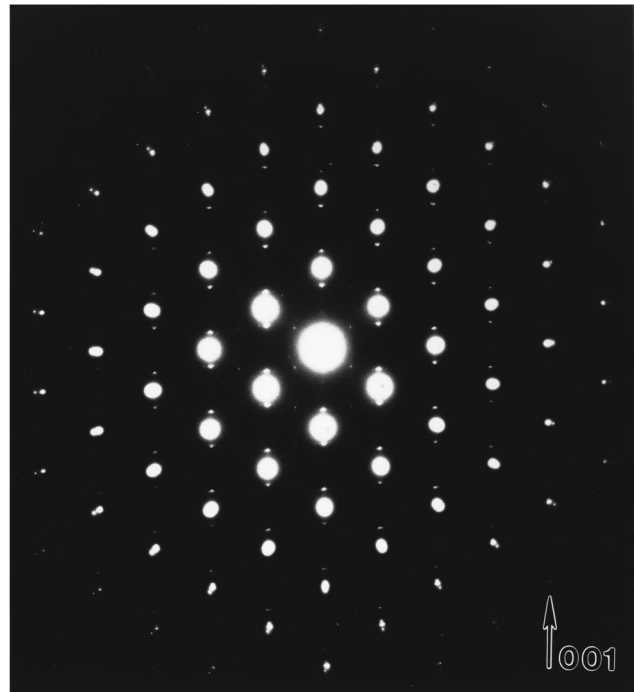


FIG. 2. A selected-area diffraction pattern taken from sample *B2215* in a [110] zone axis. Several order of superlattice reflections are easily seen. This is direct proof of that folding of the Brillouin zone has occurred.

This diffraction from the superlattice is direct proof that electron behavior is affected by the superlattice periodicity. In areas of high threading dislocation density, the periodic stacking of Si and Ge is locally perturbed, as revealed by the lateral layer undulations. We found that the amplitude of such undulations generally decreases toward the cap layer. Our earlier high-resolution TEM investigations showed that layer undulations are connected with changes in the lattice-site occupation from Si to Ge along individual {100} planes. These changes can be attributed to steps at the Si-Ge interfaces with step heights of one or a few atomic layers.^{12,13}

Quantitative analyses of the strain, composition, and structure were made using selected area diffraction. The average lattice parameters both in plane (\mathbf{a}_{\parallel}) and in the direction of the superlattice (\mathbf{a}_{\perp}) the lattice strain (ϵ) and the composition of the buffer and superlattice have been quantified. Moreover, the superlattice period and number of monolayers per Si or Ge atom for the superlattice were determined. In Table II we show a series of results for samples *B2212–B2215*. It can be seen that the superlattice structures are somewhat richer in Ge by comparison with the nominal structure. Thus, the sample *B2212* was found to have a structure that is closer to Si-Ge (4:5) than the Si-Ge (4:4) nominal structure. This tendency is uniformly seen in all samples, so we will refer to samples by their nominal structure for clarity.

Examination of the data in Table II shows that the partially relaxed buffer layer is a template which has the lattice parameter of an unstrained $\text{Si}_{0.5}\text{Ge}_{0.5}$ alloy. Samples *B1585* and *B2211*, which are $\text{Si}_{0.5}\text{Ge}_{0.5}$ alloys, are grown nearly strain free on this substrate. We can therefore directly compare the optical-absorption properties of these samples to the

TABLE II. a_{\parallel}^b and a_{\perp}^b are the lattice parameters parallel and perpendicular to the plane of epitaxy. Note that the lattice parameter in the plane of the substrate is close to that of an unstrained $\text{Si}_{0.5}\text{Ge}_{0.5}$ alloy ($a_0 = 0.555$ nm). The measured lattice parameter of the superlattices perpendicular to the substrate is also quite close to 0.554 nm, demonstrating that the average strain over one superlattice period is quite small. Strain $\epsilon_{\parallel}(\%) = 100(a_{\parallel} - a_0)/a_0$ (a_0 is the bulk lattice parameter). Λ^{SL} is the superlattice period. y is the average atomic concentration of Ge. $y_{\text{EDS}}^{\text{SL}}$ is the Ge concentration measured by electron microprobe energy dispersive spectroscopy.

Si _{1-y} Ge _y buffer					Superlattice: Si-Ge ($m:n$)							
Sample	a_{\parallel}^b nm	a_{\perp}^b nm	ϵ_{\parallel}^b %	y_{calc}^b	Λ^{SL} nm	a_{\perp}^{SL} nm	$\epsilon_{\parallel}^{\text{SL}}$ (%)	$m+n$	m	n	$y_{\text{calc}}^{\text{SL}}$	$y_{\text{EDS}}^{\text{SL}}$
B2212	0.558	0.561	-0.26	0.71	1.24	0.553	0.52	9.0	4.3	4.7	0.52	0.53
B2213	0.556	0.561	-0.36	0.66	1.51	0.553	0.30	10.9	5.4	5.5	0.50	0.51
B2214	0.555	0.556	0.0	0.52	1.50	0.554	0.10	10.8	5.1	5.7	0.53	0.52
B2215	0.557	0.561	-0.45	0.70	1.81	0.554	0.28	13.1	6.3	6.8	0.52	0.50

results of Ref. 14 on unstrained, bulk Si-Ge alloys. The superlattice samples B2212–B2215 are grown on this substrate with an average strain that is quite modest ($e < 0.6\%$) compared to the strain between adjacent Si and Ge layers ($e > 4\%$). This reduced level of strain permits the growth of layers up to several microns in thickness before the critical thickness limit is reached. The strain between adjacent Si and Ge layers is maintained at close to 4% regardless of the superlattice structure.

C. Structural analysis by transmission electron microscopy—specific samples

Samples with thin buffers (B2212 and B2213)

The interfaces between the SiGe alloy buffer and Si substrate are found to be of good planarity, while interfaces between the buffer and superlattice are undulated. Only close to the buffer are such undulations correlated with the roughness of the buffer-superlattice interface. Values for the average lattice parameters, the lattice strain, and the average composition of the buffer were determined from selected area electron diffraction and are summarized in Table II. It can be concluded from these data that partial strain relaxation of the buffer layers has occurred for all samples. TEM contrast analyses show that the strain relaxation of the Si-Ge buffer layers occurs by formation of a network of misfit dislocations, by planar defects, frequently in the form of microtwins, and by threading dislocations emerging from the substrate-buffer interface. The planar defects were identified by high-resolution lattice imaging as isolated stacking faults or as groups of stacking faults on $\{111\}$ lattice planes.

The Si-Ge (5:5) superlattice on a thick buffer (B2214)

For growth on a 1000-nm-thick buffer (sample B2214), considerable differences compared to growth on thin buffers (for example, sample B2213) are observed concerning defect densities and morphology of the superlattices. The thicker buffer layer reduces the average values for threading dislocation densities in the superlattice region by about one order of magnitude, and the density of planar defects by more than four orders of magnitude. We found the buffer of this structure to be strain relaxed, that is, $\mathbf{a}_{\parallel} = \mathbf{a}_{\perp}$. A feature only observed in this sample is a high density of small inclusions within the superlattice region that lead to localized lattice distortion. We have not yet been able to identify the nature of these inclusions.

D. Sample preparation for photoconductivity measurements

All samples were cleaned using trichloroethane, acetone, and methanol. The native surface oxide was removed using a mild buffered oxide etch (6::1HF::NH₃F). Samples were then loaded into an evaporation chamber where four 1-mm² aluminum pads 5000 Å in thickness were deposited by thermal evaporation through a shadow mask. After annealing the contacts at 425 °C, we observed that Al forms a shallow pn junction in moderately doped n -type samples. All samples were characterized for both Ohmic behavior and series resistance by means of four-point current-voltage measurements at room temperature and at 4.2 K. We found that we could obtain repeatable Ohmic contacts only if Al contacts were not annealed after the evaporation. The Ohmic nature of the contacts is due mainly to the highly doped Si cap-layer.

Samples used for optical absorption or transmission studies were not contacted. Instead, a section of the sample was removed by wet chemical etching using 6% HF-HNO₃, by volume at room temperature. The etch depth was measured using a stylus profilometer. This preparation made it possible to measure the transmission through the Si substrate, and subsequently the transmission through the same substrate and the epitaxial superlattice layer combination in order to extract the absorption coefficient.

III. OPTICAL SPECTROSCOPY

A. General considerations for absorption and photocurrent measurements

In these experiments we sought to compare the optical-absorption response of a series of superlattices all having the same average composition of 50% Si and 50% Ge by atomic percent. In addition, we have also examined the behavior of some $\text{Si}_{0.5}\text{Ge}_{0.5}$ alloys grown under similar conditions to those used to produce the superlattices. We measured the optical response of these samples using both photocurrent spectroscopy and optical transmission spectroscopy.

Photocurrent spectroscopy has the principal advantage that the photocurrent which results from absorption of photons is resolved against a rather small background. Furthermore, the signal increases as the strength of the absorption increases. However, this method cannot be used to determine the absolute value of the absorption coefficient unless the absolute quantum efficiency, taking into account reflections, can be determined. In optical transmission measurements,

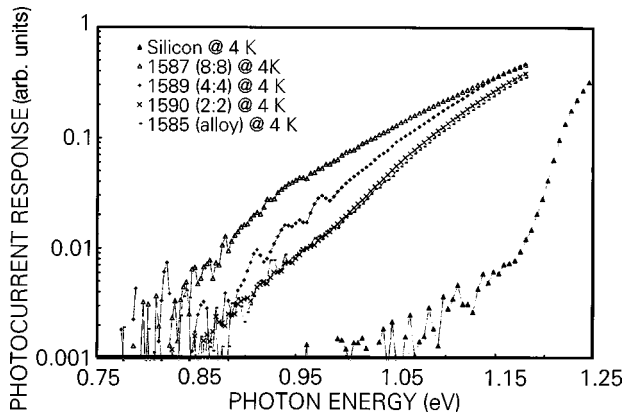


FIG. 3. Photocurrent spectra taken at 4 K for the *B15xx* series of samples. In this figure it can be seen that the *B1587* sample [a Si-Ge (8:8) superlattice] has the longest wavelength photocurrent threshold, while the $\text{Si}_{0.5}\text{Ge}_{0.5}$ alloy (*B1585*) has the shortest wavelength threshold. Note that the photocurrent spectrum for the alloy has a distinct two-component nature that is easily resolved in these data.

the signal is extracted from a larger background of unabsorbed light. In the region of high absorption, it is difficult to measure either transmission or reflection accurately. While the range of the absorption measurement is more narrow than for the photocurrent measurement, it is possible to determine an absolute magnitude for the absorption coefficient.

B. Photocurrent spectroscopy

Photocurrent spectra were recorded using phase-sensitive detection and a low-noise preamplifier in close proximity to the cryostat. Particular attention was paid to improving the signal-to-noise ratio by minimizing the length of the wiring and by careful electrical shielding. Si and GaAs filters were used to eliminate second-order transmission. The absolute optical throughput of the system was calibrated using an ILX-6810B photometer. Photocurrent spectra were taken at 300, 77, and 4 K with the sample mounted on a copper cold finger.

We had the option to measure the photocurrent perpendicular to the superlattice growth plane or the photocurrent parallel to the superlattice layers. We chose this latter configuration in order to reduce the effect of unwanted signals from the substrate. The photocurrent signal increases by three orders of magnitude between the band-gap energy and the onset of absorption by the Si substrate. The threshold energy is determined during the fitting of Eq. (4) to the measurement. Data for the 1500 series are shown in Fig. 3. Here it is easily seen that sample 1587, composed of 8 ML of Si and 8 ML of Ge, has the lowest apparent band gap. Sample 1589, with a Si-Ge (4:4) structure has the next lowest band gap, while sample *B1590*, the (2:2) superlattice, and, *B1585*, the $\text{Si}_{0.5}\text{Ge}_{0.5}$ alloy, appear to be indistinguishable. Thus these photoconductivity spectra can be used to distinguish superlattices from the each other, even though the average composition is the same. Closer examination of the curves in Fig. 3 reveals a two-threshold behavior to the photocurrent that is most easily seen for sample *B1585*, the Si-Ge alloy. The stronger of the two components has a threshold of 0.98 eV. This corresponds to the band-gap energy of the un-

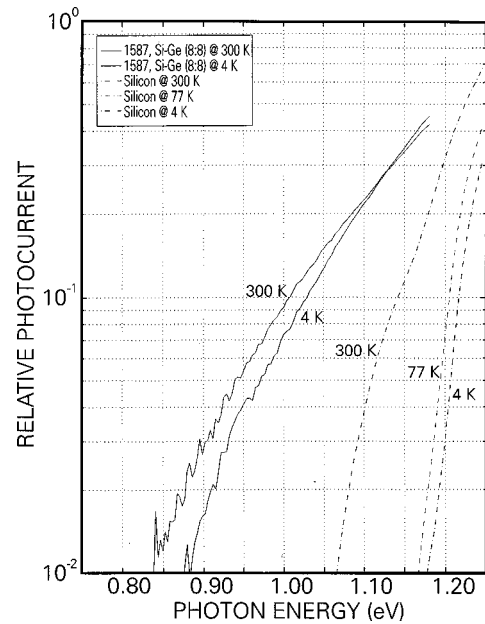


FIG. 4. The temperature dependence of the photocurrent spectra is weak when compared to that of bulk Si. The photocurrent spectra of the *B1587* sample [a Si-Ge (8:8) superlattice] is compared to Si at 300, 77, and 4.2 K. The measured shift of the threshold between 300 and 4 K is 70 meV for Si, but only 10 meV for the superlattice.

strained alloy. The lower-energy term at 0.8 eV is therefore absorption either from an impurity or a defect level in the alloy material. Similar two-component behavior is not so clearly resolved in the photocurrent spectra of the 4:4 and 8:8 superlattices.

The temperature dependence of the photocurrent spectra of superlattices is much weaker than that measured in bulk Si as shown in Fig. 4. Here we measure a significant difference between the behavior of Si, where the absorption edge shifts by 100 meV between 300 and 77 K, while, for the superlattices, this shift is much smaller, on the order of 20 meV.

In Fig. 5 we show the results measured at 77 K for two superlattices 2213 and 2214, each composed of 5 ML of Si and 5 ML of Ge. The superlattice thickness of 254 nm is the same for each. The samples differ in the thickness of the buffer regions: 2213 has a buffer thickness of 50 nm, while 2214 has a thickness of 1000 nm. The two measured absorption curves are quite similar. The spectrum of the 2212 sample, with a structure of 4 ML of Si and 4 ML of Ge, is easily distinguished from these two: notably the absorption threshold energy is higher. There are two important results that can be drawn from these experiments: (1) two different superlattices, having the same 5:5 nanostructure, but grown under different conditions, are seen to have similar photocurrent spectra; and (2) two superlattices differing by only two atomic monolayers per period (5:5) versus (4:4) are easily distinguished by the photoconductive spectrum near the band edge. The photoconductivity measurements demonstrate three important features of optical absorption by these Si-Ge structures.

(1) The onset of photoconductivity has an energy dependence that is related to the period of the superlattice. As the period of the superlattice increases, the energy of the onset decreases. These measurements can be used to distinguish

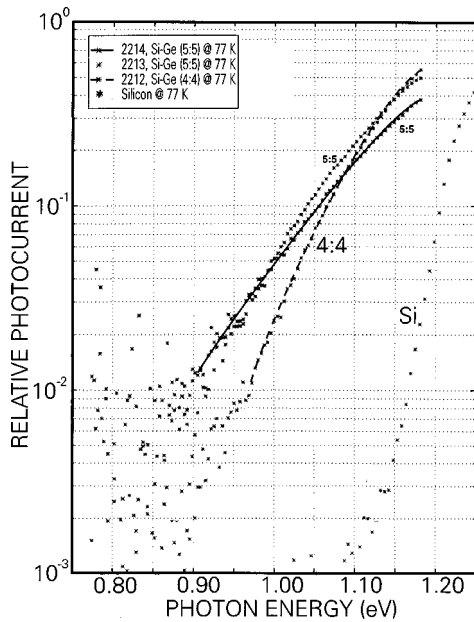


FIG. 5. Two Si-Ge (5:5) superlattice samples (*B2213* and *B2214*) are compared with one Si-Ge (4:4) structure (*B2212*). The spectra of the (5:5)-ML superlattices converge on one absorption threshold energy (0.75 eV), while the (4:4) superlattice has a distinctly larger threshold energy of 0.86 eV. This result confirms that the main characteristics of our photocurrent spectra are reproducible to the point that we can distinguish superlattice structures that differ by only two atomic monolayers per period.

two superlattice structures having the same average composition, but having a period length that is different by only two atomic monolayers.

(2) The temperature dependence of the onset of photoconductivity in superlattices is much weaker than that of silicon.

(3) The spectra of the Si-Ge alloy and the Si-Ge (2:2) superlattices are indistinguishable. This suggests that interfacial disorder is at least ± 1 atomic monolayers, but less than ± 2 atomic monolayers, since the Si-Ge (4:4) superlattice is easily distinguished from the Si-Ge (5:5) superlattice.

C. Absorption measurements by optical-transmission spectroscopy

Optical absorption spectra were taken at room temperature over the wavelength range $0.5 \text{ eV} < \hbar\omega < 1.0 \text{ eV}$ on seven samples including both Si-Ge alloys and superlattices. All measurements reported here were taken at 300 K. Samples were prepared so that differential transmission measurements could be used to extract the superlattice absorption. The sample was chemically etched to expose the substrate. Measurements of transmission were made first on the superlattice plus substrate combination, and then on the transmission through the substrate alone, immediately adjacent to the first measurement. The method described in Ref. 15 was used to minimize the effects of surface roughness on the determination of the absorption coefficient. Our measurements of samples *B2208*–*B2211* have been described in an earlier publication.^{16,17} Samples *B1587*–*B1590* were measured both in optical transmission and optical absorption spectroscopy. The differential transmission between the substrate alone and the substrate plus superlattice is nonzero for

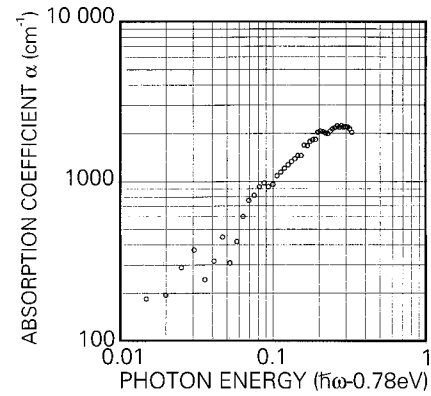


FIG. 6. Log absorption coefficient as a function of log photon energy for sample *B1587*, a Si-Ge (8:8) superlattice sample. Data were taken at 300 K. Absorption data can be resolved up to 1.0 eV.

the wavelength range $0.7 \text{ eV} < \hbar\omega < 1.0 \text{ eV}$. For a sample with an absorption threshold near 0.8 eV, we could analyze data up to about 1.0 eV in photon energy. For energies higher than this, the onset of absorption from the Si substrate quickly reduces the signal to below the noise level. The maximum differential transmission of the substrate alone was measured to be about 2% greater than the superlattice plus substrate combination for most samples. Under these conditions, we were able to measure the differential transmission spectrum over about one order of magnitude of transmitted intensity. This is two orders of magnitude less range than the photocurrent measurements described in the previous section. The experimental data were analyzed using Beer's law to determine the absorption coefficient.

Our experimental results are shown in Figs. 6–9, where the log of the absorption coefficient is plotted versus the log of (photon energy minus the band-gap energy). These data were taken over a range of photon energy from the infrared ($\hbar\omega = 0.5 \text{ eV}$) to the onset of absorption by the Si substrate ($\hbar\omega = 1.0 \text{ eV}$). The band gap was determined from the data as the lowest energy at which there was no longer a measurable difference (i.e., < 1 part in 1000) between the optical transmission through the substrate and the optical transmission through the combination of the substrate and superlattice.

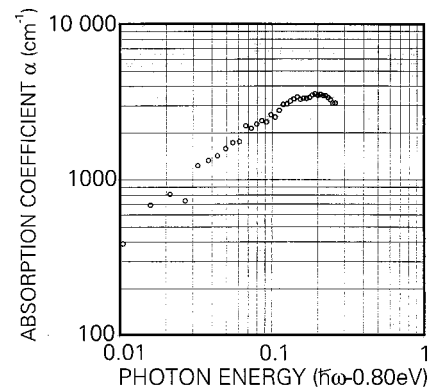


FIG. 7. Log absorption coefficient as a function of log photon energy for sample *B1589*, a Si-Ge (4:4) superlattice sample. Data were taken at 300 K. Absorption data can be resolved up to 1.0 eV.

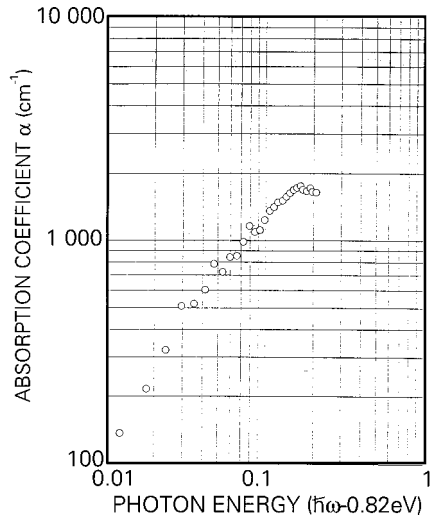


FIG. 8. Log absorption coefficient as a function of log photon energy for sample *B1590*, a Si-Ge (2:2) superlattice sample. This sample appears to be quite similar to a $\text{Si}_{0.5}\text{Ge}_{0.5}$ alloy. Data were taken at 300 K. Absorption data can be resolved up to 1.0 eV. The threshold resolved here corresponds to the deep level resolved in the photocurrent spectrum shown in Fig. 14.

The data of the *B1587–B1590* series show a progression from shorter wavelength threshold to longer wavelength threshold as the superlattice period increases. The absorption coefficient at 100 meV above the band gap is generally about 1000 cm^{-1} . The absorption coefficient for Si is about 50 cm^{-1} , while that of GaAs is about $12\,000\text{ cm}^{-1}$ under the same conditions.^{18,19} These optical transmission data confirm that there is measurable optical absorption in the Si-Ge superlattices and alloys. The value of the exponent x in Eq. (4) is equal to the slope of the absorption coefficient plotted versus photon energy on a log-log scale. In these results the dependence of the absorption coefficient on energy can be described by a linear relationship because $x \approx 1$.

In Fig. 9, we show the absorption coefficient for sample *B2208* which has a nominal (4:4) composition. In a previous publication we reported a band gap of 0.71 eV and an absorption coefficient of $7,000\text{ cm}^{-1}$ at 100 meV above the band gap.¹⁷ The results presented in Fig. 9 for the same

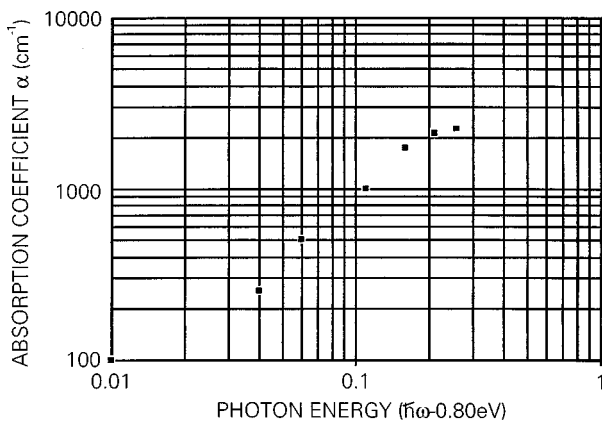


FIG. 9. Absorption coefficient vs photon energy for sample *B2208*, a Si-Ge (4:4) superlattice structure grown on a thin buffer layer. Data were taken at 300 K. Absorption data can be resolved up to 1.0 eV. The band gap of the sample is 0.8 eV.

sample were taken from independent measurements in a different laboratory, with particular attention paid to the optical quality of the sample surfaces. The substrate surface of *B2208* was thinned and optically polished in order to reduce diffuse scattering of light incident on the sample. The analysis of the absorption experiment gives a larger band gap (0.8 eV) and a smaller absorption coefficient (1000 cm^{-1}) than our previously reported values for the same sample. These results illustrate that the quality of the sample surfaces is important even when differential spectroscopy is used to minimize the contribution of the substrate, including its surface quality, to the absorption spectrum.

Optical-transmission experiments permit the analysis of the behavior of the absorption coefficient between 0.6 and 1.0 eV. Compared to the results obtained in photoconductivity, there are four important findings in these experiments (See Table III).

(1) The determination of the band-gap energy by optical-absorption spectroscopy is only in approximate agreement with that determined in photoconductivity measurements. The largest difference is about 20%.

(2) The trend that the band gap decreases with increasing superlattice period is found in both photoconductivity and absorption measurements.

(3) The absorption coefficient inferred from these measurements increases linearly with photon energy, in distinct contrast with the behavior of photoconductivity.

(4) The reproducibility of these absorption measurements is not sufficiently good enough to discriminate one superlattice structure from another, unlike our photocurrent measurements.

IV. THEORETICAL DETERMINATION OF THE ABSORPTION COEFFICIENT

The theoretical determination of the absorption coefficient was achieved using an empirical tight-binding method that has been adjusted to give excellent agreement for the optical properties of bulk Si and Ge.^{9,20,21} The basis set uses sp^3 orbitals, in the three-center representation, with spin-orbit coupling included. The method has been tested successfully by calculation of the deformation potentials and optical properties of Si-Ge superlattices.⁹ The absorption coefficient depends mainly on the joint density of states which is deduced directly from the band structure. We have considered only direct interband transitions to determine the absorption coefficient. This procedure tends to underestimate the absolute magnitude of the absorption coefficient by ignoring the contribution from indirect transitions, which may be substantial in short-period superlattice materials like these. The most important aspect of the calculation is that the optical properties are integrals over the Brillouin zone, and the integration method used in the present calculations is the very successful linear analytic tetrahedron method.

The calculation of the bandstructure can be used to determine the band gap of a series of Si-Ge ($n:n$) superlattices as a function of the number of monolayers per period. The results of these calculations are shown in Fig. 10 along with the experimental data taken by photocurrent spectroscopy. Both theory and experiment show the same trend, namely, that the band gap of the superlattices decreases as the length

TABLE III. Results of optical transmission measurements of Si-Ge superlattices and alloys.

Sample	Nominal composition	E_g @ 300-K band gap (eV)	α absorption coefficient @ 100 meV above E_g	Dependence of α on photon energy
B1587	8:8	0.78	1000 cm ⁻¹	linear
B1589	4:4	0.80	2500 cm ⁻¹	$(\hbar\omega)^{0.7}$
B2208	4:4	0.80	1000 cm ⁻¹	linear
B1590	2:2(alloy)	0.82	1200 cm ⁻¹	linear

of the supercell period increases. This finding confirms earlier observations of Menczgar *et al.*²² and Olajos *et al.*²³ In Fig. 10, the calculated band gaps correspond to the filled diamonds. The calculated points are joined by a broken line to guide the eye, and distinguish them from measurements that are shown as open squares and circles. Theory and experiment are in agreement on the trend of the band gap, but do not agree on the amount of the change. The dependence of the calculated band gap on superlattice period shows a 40% decrease between the value for the Si-Ge alloy and the Si-Ge (8:8) superlattice. The measured change in photoconductive measurements (open squares) is only about half this amount. The absorption measurements (open circles) indicate a 5% percent decrease.

Our calculations show that the optical absorption coefficient for superlattice structures is enhanced over that of the alloy of the same average composition. This result can be understood from the following schematic analysis. The top of the valence band in Si-Ge alloys has p -type symmetry. The conduction-band minima along the $\langle 100 \rangle$ directions also have p -type symmetry. Direct optical transitions between the valence and conduction bands at the band edge are forbidden by symmetry. Superlattice structures of Si and Ge that have a period of about 1 nm experience a folding that brings the minimum of the conduction band to center, i.e., to $\mathbf{k}=0$, of the Brillouin zone. The folded states are derived from the indirect bandgap states that lie along the axis of the super-

lattice, and maintain much of their original p -type character. In addition they will interact and mix with the direct-band-gap states that lie about 2.5 eV above the valence-band edge. The latter states have an s -type character, and wave-function mixing will introduce s -type character into the zone-folded superlattice states, leading to allowed direct optical transitions in Si-Ge superlattice structures. The perturbation that mediates the mixing of the folded states with the s -type conduction states comes from the difference in atomic potentials between Si and Ge, and from the fraction of the unit cell occupied by Si and Ge. An additional perturbation is generated by interfacial disorder. Strozier *et al.* showed that introduction of interfacial disorder into a short-period superlattice results in an increase in the optical transition rate across the band gap.²⁴ Thus folding of the Brillouin zone introduces a new density of states at $\mathbf{k}=0$, while the differences in the atomic potential caused by chemistry (Ge versus Si) specify the magnitude of the optical matrix element.

The calculations presented here take into account only the absorption due to direct transitions across the gap. Measurements, on the other hand, include contributions from direct transitions, and also from indirect transitions between non-folded states. It is therefore expected that experimental measurements of absorption coefficient will exceed the theoretical calculated values. The imaginary part of the dielectric function is calculated by the relation

$$\epsilon_2(\omega) = \frac{4\pi^2 e^2}{m^2 \omega^2} \sum_{c,v} \int \frac{2}{(2\pi)^3} |\langle \mathbf{k}, c | \mathbf{P} \cdot \mathbf{a} | \mathbf{k}_1, v \rangle|^2 \times \delta[E_{cv}(k) - \hbar\omega] d^3k, \quad (5)$$

where $|\mathbf{k}, c\rangle$ and $|\mathbf{k}, v\rangle$ stand for the wave functions of the conduction and the valence bands, respectively, and $E_{cv}(k)$ for the energy difference between the conduction (c) and valence (v) bands. \mathbf{P} is the momentum operator and \mathbf{a} the polarization unit vector. The absorption coefficient $\alpha(\omega)$ is then obtained by the relation

$$\alpha(\omega) = \frac{\epsilon_2(\omega)\omega}{cn(\omega)}, \quad (6)$$

with $n(\omega)$ the refractive index and c the speed of light. In addition to ideal superlattices, calculations were also done for superlattices with an intermixing of the atoms at the interface. In the present calculation, the interface intermixing was modeled with the first atomic layer at each site of the interface containing 50% Ge atoms and 50% Si atoms, while the second containing 75% atoms of the host material and

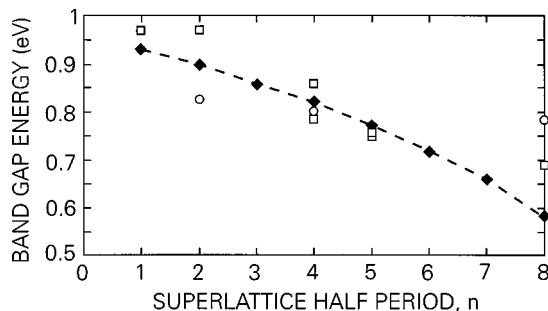


FIG. 10. Theoretical determination of the band gap of SiGe ($n:n$) superlattices for different superlattice half-periods (n). The calculated values are designated by the closed diamonds. The dotted line is intended to guide the eye. These calculations are compared to experimental results derived from the photoconductive threshold. Experimental results are indicated by the open squares for photoconductivity measurements, while the open circles show the results of absorption measurements. Note the much weaker dependence of absorption measurements on superlattice period compared to either photoconductivity measurements or theory, which shows the strongest dependence.

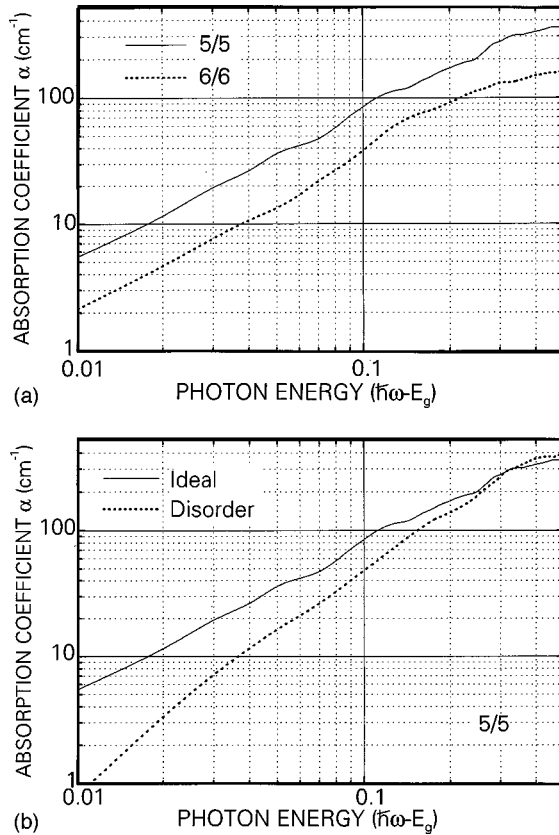


FIG. 11. Theoretical determination of the absorption coefficient on energy for several Si-Ge ($n:n$) superlattice structures. (a) The absorption coefficient of a Si-Ge (5:5) superlattice (solid line) is two times larger than that for a (6:6) superlattice. This difference can be related to the density of states at the center of the Brillouin zone. (b) The absorption coefficient for a Si-Ge (5:5) superlattice with atomically perfect interfaces is compared to that for the same structure with atomically rough interfaces. This disorder changes the functional dependence of the absorption coefficient from a linear to a quadratic dependence on photon energy.

25% atoms of the second material. The atoms at the interface were randomly placed, and the calculations were done with a supercell.²¹

In Fig. 11 we show two aspects of the dependence of the absorption coefficient on superlattice structure. In Fig. 11(a) we compare the calculated absorption coefficient for ideal Si-Ge (5:5) and Si-Ge (6:6) superlattice structures. The figure shows, in a log-log plot, the absorption coefficient versus the photon energy above the band gap E_g . The two curves are similar, showing a near-linear dependence of the absorption coefficient on the photon energy. The strength of the absorption coefficient for the Si-Ge (5:5) structure exceeds that of the (6:6) structure by a factor of 2 over the range of the calculation. This difference is a result of the different zone folding produced by the superlattice symmetry. The (5:5) superlattice results in the maximum density of states at the zone center due to the fact that the minimum in the conduction band of the unfolded Si-Ge alloy occurs at $\mathbf{k} = 0.8\mathbf{k}_{zb}$, where \mathbf{k}_{zb} defines the Brillouin-zone boundary. A five-times folding of the Brillouin zone brings this minimum to $\mathbf{k} = 0$. Note that the absorption coefficient reaches a level of about 100 cm^{-1} at 100 meV above the band gap. When compared with the experimental values, the strength of the

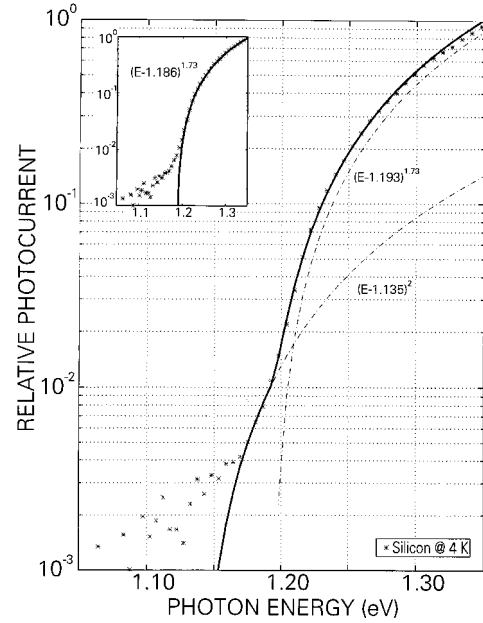


FIG. 12. Analysis of the photocurrent spectrum for Si. An expression of the form: $A(E - E_g)^x$ is fit to the data. A two-term fit yields both the band gap $E_g = 1.19 \text{ eV}$ and the optical-phonon energy of 0.58 eV for Si.

absorption coefficient remains at about one order of magnitude less than the measured values. The absorption coefficient rises linearly with photon energy as observed in transmission measurements, but not as seen in photoconductivity spectra.

Interfacial disorder affects the absorption near the band edge. Figure 11(b) shows, for comparison, the absorption coefficient of the ideal (5:5) superlattice, as well as that of superlattice 5:5 with disordered interfaces. The strength of absorption for the disordered superlattice is lower near the band edge and the absorption coefficient departs from the linear behavior calculated for perfect superlattice structures. The absorption coefficient increases with nearly the square of the photon energy. These modifications are mainly caused by the modification of the density of states, and the net effect is to broaden the energy width of the absorption edge, and increase the exponent x in Eq. (4).

V. ANALYSIS OF PHOTOCURRENT DATA

The photocurrent spectra, in contrast to results obtained by transmission spectroscopy, show a clear nonlinear dependence on photon energy. To characterize this dependence, we fit an expression of the form of Eq. (4) to the data to determine both the band gap and the exponent. This procedure was evaluated first by analyzing the photocurrent spectrum. These results are shown in Fig. 12 for measurements taken at 4 K. The inset shows the result of a least-squares fit to all the data above 1.2 eV: $E_g = 1.19 \text{ eV}$ and $x = 1.7$. The value for the band-gap energy is in excellent agreement with the accepted value for Si at 4 K. The exponent $x = 1.7$ is determined from this procedure. In the principal part of Fig. 12, we have included an additional term to fit the tail in the photocurrent spectrum beyond 1.2 eV. This analysis does not change the values for the band gap, but identifies an addi-

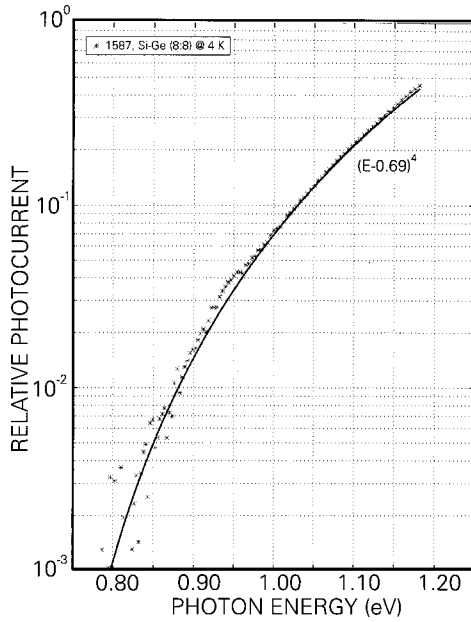


FIG. 13. Single-threshold fit to 1587. The band gap is determined to be 0.69 eV with an exponent $x=4$.

tional transition at 0.058 eV below the band edge. The energy is equal to the optical-phonon energy in Si.

We have fit all of the measured spectra to a single curve of the form of Eq. (4). To use this approach we are making the assumption that the optical absorption can be modeled as a transition between a single level in the valence band to a single level in the conduction band as is the case in elemental Si. The result of this fitting gives a band-gap energy and the exponent of the dependence of the photocurrent on photon energy. These results can be compared to similar analyses published in earlier experimental and theoretical work.

Photocurrent spectra

Raw photocurrent data were first corrected for the monochromator throughput and for the noise floor at lower energies. The data can then be analyzed over about three decades of photoresponse. At 4 K, this corresponds to an energy range of $0.7 \text{ eV} < E < 1.2 \text{ eV}$. Using a single-threshold model for absorption based on Eq. (4), we found that the best agreement is obtained when the exponent $x \approx 4$. At the present time there is not an explicit theoretical model that justifies

the use of $x=4$. However, we can demonstrate theoretically that the presence of defects and disorder, for example, will increase the exponent that characterizes absorption near the band gap. In Fig. 13, we show the result of such a fitting for sample B1587, a Si-Ge (8:8) superlattice. Through this fitting procedure, we can extract the threshold energy for the photocurrent of 0.69 eV. A similar analysis has been performed for all samples studied in this work.

Our measurements are summarized in Table IV along with the results of Olajos *et al.*,²³ who examined some of the same samples, as well as our theoretical calculations of these superlattices. It can be seen that the band gap decreases monotonically as the superlattice period increases in both experiment and theory. The average compositions for all superlattices and alloys are the same: 50% Si and 50% Ge. In the cases, where our measurements can be compared directly to those of Ref. 23, there is agreement within 10 meV for the value of the band gap. In two cases we can also compare the band gaps of samples having the same nominal structure, but grown at different times under different conditions. In the case of samples B2213 and B2214, the absorption spectra by photocurrent are nearly indistinguishable, and yield the same value for the bandgap within 10 meV. Samples B2212 and B1589 have a nominal 4:4 structure. In this case the values of the band gap differ by about 70 meV, which is well outside the margin of error for the measurements. Strain in the superlattice will also change the band gap. The presence of an increase in the Ge layer thickness from the nominal thickness of 4 means that the strain will no longer be symmetrically divided between the Si and Ge layers. Zachai *et al.* showed that strain resulting from excess Ge layers in these short-period Si-Ge superlattices will reduce the band gap.²⁵ The difference in the band gap between these two samples may be due to such an effect.

In the case of sample B1590, there is an apparent difference between the band gap measured by optical transmission and that measured in photoconductivity. The photoconductivity spectrum for sample B1590 is shown in Fig. 3, and is seen to be identical to that for the Si-Ge alloy, sample B1585. Analysis of this sample shows clearly two components to the spectrum: one at 0.97 eV that we identify with the band gap, and a deep level at 0.79 eV, as shown in Fig. 14. The optical-transmission spectrum can be taken up only to 1.0 eV, and therefore does not permit resolution of the higher-energy feature seen in photoconductivity. Analysis of

TABLE IV. Summary of single-threshold band-gap calculations and measurements on Si-Ge superlattices and alloys.

Sample No.	Composition	4-K band gap (eV) from			Band gap (eV) from Ref. 24
		Theory	photocurrent	Absorption	
B1585	Si _{0.5} Ge _{0.5}	0.93	0.97		
B1590	Si-Ge (2:2)	0.90	0.97	0.82	
B1589	Si-Ge (4:4)	0.82	0.79	0.80	
B2212	Si-Ge (4:4)	0.82	0.86		0.85
B2213	Si-Ge (5:5)	0.78	0.75		
B2214	Si-Ge (5:5)	0.78	0.76		0.76
B1587	Si-Ge (8:8)	0.58	0.69	0.78	

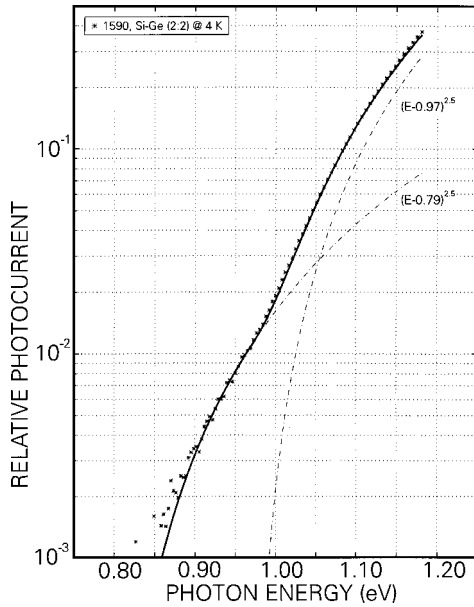


FIG. 14. Analysis of the photocurrent spectrum of sample B1590. This sample has a nominal (2:2) structure, but due to interfacial roughness of ± 1 ML is indistinguishable from a Si-Ge alloy. The data mandate a two-term fit which yields the band gap of 0.97 eV and a deep level at 0.79 eV.

the transmission data therefore gives only the characteristics of the deep-level absorption in sample B1590.

VI. DISCUSSION AND CONCLUSIONS

In this paper we report on a study of the dependence of optical properties of Si-Ge ($n:n$) superlattices on superlattice nanostructure. The samples were grown on (001) Si as symmetrically strained superlattices on partially strain-relieved buffer layers. All structures could be synthesized with a thickness of at least 200 nm, so that the measured optical properties are representative of fully three-dimensional macroscopic Si-Ge synthetic crystals. This study coordinates materials growth, analysis by TEM and optical spectroscopy. A principal objective of this study is the comparison of the experimental and theoretical determination of the dependence of optical absorption on incident photon energy.

Optical absorption was measured by photoconductivity and by direct optical transmission. The dependence of the photoconductivity signal in the superlattices on photon energy can be expressed as $I(\hbar\omega) = I_0(\hbar\omega - E_g)^4$ over three orders of magnitude of photocurrent for $0.6 \text{ eV} < \hbar\omega < 1.2 \text{ eV}$. The threshold energy for photoconductivity can be used to distinguish superlattices of the same average composition by their period. In these experiments we could easily distinguish the photoconductivity spectrum of a Si-Ge (4:4) superlattice from that of a Si-Ge (5:5) structure. These two superlattices differ by only two atomic monolayers per period. This result implies that interfacial roughness is less than ± 2 ML. The superlattice with the shortest period measured in these experiments was a Si-Ge (2:2) structure. The optical-absorption spectrum of this sample was seen to be indistinguishable from that for a $\text{Si}_{0.5}\text{Ge}_{0.5}$ alloy, implying that the level of interfacial roughness and disorder is on the order of at least ± 1 atomic monolayer.

Differential optical transmission spectra were taken at 300 K in the energy range between 0.6 and 1.0 eV. The absorption coefficient was deduced by comparison of the transmission through the combination of the substrate and superlattice to transmission through the substrate alone. The results of these measurements give threshold energies for photon absorption that are in approximate agreement with values obtained in photoconductivity experiments. However, the absorption has a linear dependence on photon energy, and this behavior is quite distinct from that measured in photoconductivity. These optical transmission data can be used to deduce the optical-absorption coefficient. Our results show that the optical absorption coefficient is on the order of $1,000\text{--}2000 \text{ cm}^{-1}$ at 100 meV above the threshold energy for absorption.

The differential transmission technique should eliminate the influence of the substrate optical properties on the optical-absorption coefficient. We tested this by measurements of transmission on different samples of the same wafer having a different surface finish on the substrate side. While these measurements show general agreement, the fluctuations in the energy threshold for absorption are significant. We measured the dependence of the band gap on the superlattice period length using transmission data. This dependence is not as strong as that measured in photoconductivity, and the fluctuations make this method less reliable than photoconductivity for a determination of the band gap.

Direct calculation of the optical-absorption properties taking into account strain and disorder was achieved using an empirical tight-binding calculation of the band structure of the specific superlattices used in our measurements. From the band-structure calculation, we determined the band gap of the superlattice, the dependence of the band gap on photon energy, the dependence of the absorption coefficient on photon energy, and the effect of superlattice disorder on this variation of absorption coefficient with energy. The value of the band gap calculated by theory is in general agreement with measurement, but the functional dependence of the band gap on superlattice period determined by our calculations is stronger than the dependence observed in the measurement, assuming that the threshold for photon absorption is the band-gap energy.

Our calculations for structurally perfect superlattices show the linear dependence of the absorption coefficient on photon energy, similar to that observed in transmission experiments. However, the effect of an interfacial roughness of 2 ML is to reduce the strength of the absorption coefficient and broaden the dependence on photon energy to a quadratic dependence. Although we are confident that the samples have an interfacial disorder of at least 2-ML thickness, we have not seen in the transmission experiments the dependence of absorption coefficient on photon energy that is expected for disordered samples.

In experimental results, we have measured a dependence of band-gap energy on superlattice structure, with the alloy structure having the largest band gap, in agreement with theory. The dependence of the band gap on the superlattice structure is a clear indication that the superlattice symmetry folds the Brillouin zone, and that this folding is sensed by conduction-band electrons. The dependence of the optical-absorption coefficient on the photon energy is a way to de-

termine whether the character of the optical transition near the band gap is direct or indirect. Our experiments show that the characters of the optical transitions for all superlattice structures are similar to each other, and similar to that for the Si-Ge alloy. Since we have shown that folding of the Brillouin zone has occurred, there is a direct transition at $\mathbf{k}=0$ in the superlattice structures. However, the energy of this transition must be close to that of the indirect-band-gap energy. Our theoretical calculations show that this energy difference is less than 100 meV at $\mathbf{k}=0$. Therefore, it is likely that the optical character of the bandgap is determined by both direct and indirect transitions.^{25,26}

The calculation of the absorption coefficient is based only on the contribution of direct transitions to the absorption. The measurements, of course, show the effects of absorption by direct transitions, indirect transitions, impurity levels, and defects. It is not surprising that the magnitude of experimentally measured absorption is larger than the calculated result. Our superlattice samples have a concentration of strain-related defects on the order of 10^{10} cm^{-2} . These defects will affect absorption differently from photoconductivity. Experimental optical-absorption spectra are a combination of intrinsic band-to-band absorption and extrinsic defect-related effects. Photoconductivity spectroscopy is an indirect measurement because the signal also depends on the subsequent diffusion of electron-hole pairs to the contacts. Thus photoconductivity, unlike absorption, may not be sensitive to photons absorbed by localized states near the band edge. Added to this is the presence of an electric field to collect the carriers. This field will enhance the infrared response by field-assisted tunneling (Franz-Keldysh effect). Photoconductivity gives a direct measure of the carriers created by absorption against a very small background, and the dynamic range is about 3–4 orders of magnitude. However, the photoconductivity measurement can give only the relative absorbance at different photon energies. Our work so far demonstrates that optical transmission spectroscopy and photocurrent spectroscopy measurements are not equivalent. Similar differences were noted by Schrottke *et al.* in their study of GaAs/Al_xGa_{1-x}As superlattices.²⁷ Finally, these considerations lead us to conclude that the optical transmission data are not sufficiently accurate to be compared quantitatively with calculated absorption spectra.

The presence of optically active direct-band-gap states near the band edge is the result of two causes. One is the

folding of indirect states to the zone center with approximately the same energy, and the second is the increase in the optical measurement due to mixing of the folded states with other states at $\mathbf{k}=0$. The essential feature of a zone-folded state is that its energy is not very different from that of the unfolded state. Thus this one-dimensional folding technique cannot be used to produce a direct-band-gap semiconductor whose direct transition energy is well separated and lower in energy from competing indirect transitions. A related effect deals with the superlattice structure itself.

Certain superlattice structures, for example those whose period consists of ten atomic monolayers, have been shown to favor a direct-band-gap band structure in theoretical calculations. In our work we have demonstrated by measurement that the superlattice period shows local fluctuations of the order of ± 1 atomic monolayer. We have, in addition, successfully distinguished two superlattices whose periods differ by only two atomic monolayers. However, we have not measured corresponding differences in the strength or behavior of absorption that might distinguish a direct from an indirect band-gap material. At this time the fluctuations in structure, while quite small, are still too large to permit the definition in experiment of the perfect superlattice structure that would possess the well-defined direct band gap that is predicted by theory.

The use of superlattice band folding as a technique to elicit direct-band-gap behavior from group-IV semiconductors was studied recently by Johnson and Ashcroft.²⁸ They examined and compared the one-dimensional superlattice ordering that we have studied in Si-Ge to three-dimensional ordering. They conclude that one-dimensional superlattices do not provide the means to create direct-band-gap superlattices whose band-gap energy is sufficiently lower than that of the indirect states to create a bona fide direct-band-gap material. The basis of this argument is quite analogous to that used by Yablonovitch to create three-dimensional photonic bandgap structures.²⁹ Their conclusion that three-dimensional ordering of group-IV can create such bona fide direct-gap materials remains an important challenge to experimental superlattice physics.

ACKNOWLEDGMENTS

We wish to express our thanks for the support of this research by the National Science Foundation Solid-State and Microstructures Program under Grant No. ECS-9210535.

*Electronic address: pearsall@maxwell.ee.washington.edu

[†]Present address: Dipartimento di Ingegneria Elettronica, Università degli Studi "Roma Tre," Via della Vasca Navale, 84, 00146 Rome, Italy.

[‡]Work performed at Institut für Festkörperforschung, D-52425 Jülich, Germany.

¹H. Presting, in *Strained-layer Epitaxy, Materials, Processing and Service Applications*, edited by E. A. Fitzgerald, J. Hoyt, K. Y. Cheng, and J. Bean, MRS Symposia Proceedings No. 379 (Materials Research Society, Pittsburgh, PA, 1995), pp. 417–431.

²B. S. Meyerson, *Sci. Am.* **270**, 42 (1994).

³B. Y. Tsaur, C. K. Chen, and S. A. Marino, *Opt. Eng. (Bellingham)* **33**, 72 (1994).

⁴J. Engvall, J. Olajos, H. G. Grimmeiss, H. Presting, H. Kibbel, and E. Kasper, *Appl. Phys. Lett.* **63**, 491 (1993).

⁵T. P. Pearsall, *Prog. Quantum Electron.* **18**, 97 (1994).

⁶J. Sturm, in *Properties of Strained and Relaxed Silicon Germanium*, edited by E. Kasper (IEE/INSPEC, London, 1993), pp. 94–102.

⁷C. Tserbak and G. Theodorou, *J. Appl. Phys.* **76**, 1062 (1994).

⁸J. I. Pankove, *Optical Processes in Semiconductors* (Dover, New York, 1971), p. 35ff.

⁹C. Tserbak, H. M. Polatoglou, and G. Theodorou, *Phys. Rev. B* **47**, 7104 (1993).

¹⁰H. M. Polatoglou, G. Theodorou, and C. Tserbak, *Phys. Rev. B* **49**, 8132 (1994).

- ¹¹E. Kasper and F. Schäffler, in *Strained-Layer Superlattices: Group-IV Compounds*, edited by T. P. Pearsall, Semiconductors and Semimetals, Vol. 33 (Academic, Cambridge, 1991), pp. 223–309.
- ¹²W. Jäger, D. Stenkamp, P. Ehrhart, K. Leifer, W. Sybertz, H. Kibbel, H. Presting, and E. Kasper, *Thin Solid Films* **222**, 2121 (1992).
- ¹³D. Stenkamp and W. Jäger, *Ultramicroscopy* **50**, 321 (1993).
- ¹⁴R. Braunstein, A. R. Moore, and F. Herman, *Phys. Rev.* **109**, 695 (1958).
- ¹⁵K. A. Epstein, D. K. Misemer, and G. D. Vernstrom, *Appl. Opt.* **26**, 294 (1987).
- ¹⁶T. P. Pearsall, C. C. M. Bitz, L. B. Sorensen, H. Presting, and E. Kasper, *Thin Solid Films* **222**, 254 (1992).
- ¹⁷T. P. Pearsall, H. Polatoglou, H. Presting, and E. Kasper, *Phys. Rev. B* **54**, 1545 (1996).
- ¹⁸W. C. Dash and R. Newman, *Phys. Rev.* **99**, 1151 (1955).
- ¹⁹M. D. Sturge, *Phys. Rev.* **127**, 768 (1962).
- ²⁰C. Tserbak and G. Theodorou, *Phys. Rev. B* **50**, 18 179 (1994).
- ²¹G. Theodorou and C. Tserbak, *Phys. Rev. B* **51**, 4723 (1995).
- ²²U. Menczigar, G. Abstreiter, J. Olajos, H. Grimmeiss, H. Kibbel, H. Presting, and E. Kasper, *Phys. Rev. B* **47**, 4099 (1993).
- ²³J. Olajos, J. Engvall, H. G. Grimmeiss, U. Menczigar, G. Abstreiter, H. Kibbel, E. Kasper, and H. Presting, *Phys. Rev. B* **46**, 12 857 (1992).
- ²⁴J. A. Strozier, Y. A. Zhang, C. Horton, and A. Ignatiev, *Appl. Phys. Lett.* **62**, 3426 (1993).
- ²⁵R. Zachai, K. Eberl, G. Abstreiter, E. Kasper, and H. Kibbel, *Phys. Rev. Lett.* **64**, 1055 (1990).
- ²⁶R. A. Höpfel, *Appl. Phys. Lett.* **51**, 106 (1987).
- ²⁷L. Schrottke, H. T. Grahn, R. Klann, and K. Fujiwara, *Appl. Phys. Lett.* **66**, 1533 (1995).
- ²⁸K. A. Johnson and N. W. Ashcroft, *Phys. Rev. B* **54**, 14 480 (1996).
- ²⁹E. Yablonovitch, *J. Mod. Opt.* **41**, 173 (1994).